Molecular Systems Biology 8; Article number 586; doi:10.1038/msb.2012.18
Citation: ***Molecular Systems Biology*** **8:586**

www.molecularsystemsbiology.com

molecular systems biology

Positive roles for negative regulators in the mating response of yeast

John R Houser[1], Eintou Ford[2], Michal J Nagiec[2], Beverly Errede[2,*] and Timothy C Elston[3,*]

[1] Department of Physics, University of North Carolina, Chapel Hill, NC, USA, [2] Department of Biochemistry and Biophysics, University of North Carolina, Chapel Hill, NC, USA and [3] Department of Pharmacology, University of North Carolina, Chapel Hill, NC, USA
* Corresponding authors. B Errede, Department of Biochemistry and Biophysics, University of North Carolina, 3043 Genetic Medicine, 120 Mason Farm Road, Chapel Hill, NC 27599-7260, USA. Tel.: +1 919 966 3628; Fax: +1 919 966 2852; E-mail: errede@email.unc.edu or TC Elston, Department of Pharmacology, University of North Carolina, 4092 Genetic Medicine, 120 Mason Farm Road, Chapel Hill, NC 27599-7365 USA. Tel.: +1 919 843 7670; Fax: +1 919 966 5640; E-mail: telston@med.unc.edu

Received 12.10.11; accepted 30.4.12

All cells must detect and respond to changes in their environment, often through changes in gene expression. The yeast pheromone pathway has been extensively characterized, and is an ideal system for studying transcriptional regulation. Here we combine computational and experimental approaches to study transcriptional regulation mediated by Ste12, the key transcription factor in the pheromone response. Our mathematical model is able to explain multiple counterintuitive experimental results and led to several novel findings. First, we found that the transcriptional repressors Dig1 and Dig2 positively affect transcription by stabilizing Ste12. This stabilization through protein–protein interactions creates a large pool of Ste12 that is rapidly activated following pheromone stimulation. Second, we found that protein degradation follows saturating kinetics, explaining the long half-life of Ste12 in mutants expressing elevated amounts of Ste12. Finally, our model reveals a novel mechanism for robust perfect adaptation through protein–protein interactions that enhance complex stability. This mechanism allows the transcriptional response to act on a shorter time scale than upstream pathway activity.
Molecular Systems Biology **8**: 586; published online 5 June 2012; doi:10.1038/msb.2012.18
Subject Categories: simulation and data analysis; signal transduction
Keywords: Dig2; perfect adaptation; protective protein complexes; Ste12; transcriptional regulation

Introduction

Recently much work has been devoted to understanding the design principles of the genetic regulatory networks used by cells to respond to changes in the extracellular environment. Many of these investigations have combined mathematical modeling with experimental investigations to establish how simple network motifs, such as feed forward or feedback loops, tightly regulate temporal patterns of gene expression. Here we use a similar approach to discover novel functions for a class of negative regulators that inhibit transcription by binding to and repressing transcriptional activators. We focus on transcriptional regulation in the mating response of *Saccharomyces cerevisiae* (yeast). This system has served as a prototypical signaling network, and many of the discoveries made from studying this pathway have borne direct relevance to signaling in human cells.

Yeast can stably propagate as haploids, existing as one of two mating types, depending on the allele at the mating-type locus (*MAT***a** or *MAT*α). Both *MAT***a** and *MAT*α cells secrete a mating-type-specific pheromone (**a**- and α-factor, respectively) that signals their presence to cells of opposite mating type. Much is known about the pathway that receives the extracellular signal and initiates a mating response. Genome-wide analysis has established the genes that are regulated during this process (Roberts *et al*, 2000). Typically, these genes contain pheromone responsive elements (PREs) in their promoter regions. The protein Ste12 is the primary transcription activator responsible for initiating the genetic program required for mating. Prior to stimulation with pheromone, Ste12 is held inactive by the negative regulators Dig1 and Dig2 (Cook *et al*, 1996; Tedford *et al*, 1997; Bardwell *et al*, 1998). Stimulation of *MAT***a** cells with α-factor leads to dissociation of Dig1 and Dig2, allowing Ste12 to initiate transcription from promoters containing PREs. Expression from promoters containing PREs is typically transient, with mRNA levels peaking at around 30 min following stimulation with pheromone before returning to near basal levels. This transient response is significantly shorter than upstream MAP kinase activity, which does not peak until around 60 min (Hao *et al*, 2008). This difference in time scales suggests a regulatory mechanism at or below the level of the MAP kinase that dampens Ste12 activity. Indeed, it has been demonstrated that Ste12 is degraded in pheromone-dependent manner (Esch *et al*, 2006). However, Ste12 is also under the regulation of four PREs, generating a positive feedback loop in the system (Zeitlinger *et al*, 2003). Additionally, Ste12 binds to another transcription factor, Tec1. In nutrient-limiting conditions, the

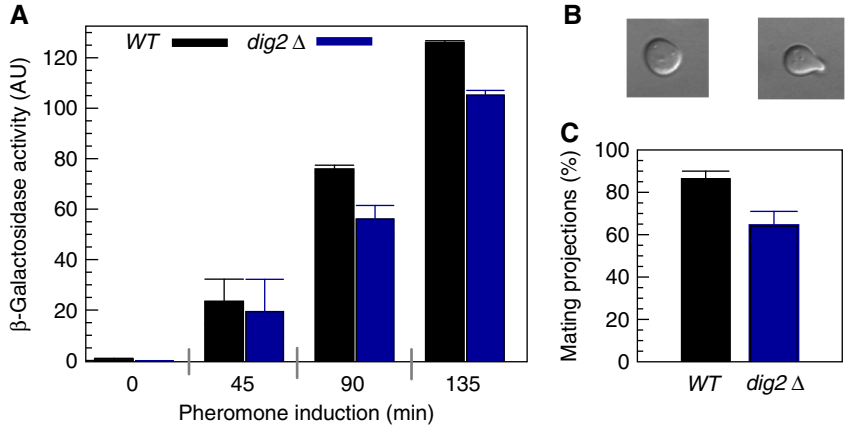

Figure 1 Dig2 has a positive role in transcriptional and morphological responses to pheromone. (**A**) Transcriptional response of a *FUS1* promoter reporter gene as measured by β-galactosidase activity following treatment with 10 μM α-factor (*WT*—black and *dig2*Δ—blue). Error bars represent standard error of the mean (**B**) Differential interference contrast (DIC) images of an unbudded vegetative cell (left panel) and a cell exhibiting a pheromone-induced mating projection (right panel). (**C**) Percentage of *WT* and *dig2*Δ cells forming mating projection following treatment with 10 μM α-factor. Error bars represent standard error of the mean. Source data is available for this figure in the Supplementary Information.

Ste12–Tec1 heterodimer is one of the key transcriptional regulators of the genetic program needed for the filamentous response (Madhani and Fink, 1997). This interaction with Tec1 further complicates the picture of transcriptional regulation by Ste12. The existence of multiple positive and negative control mechanisms makes understanding transcriptional regulation by the pheromone signaling pathway non-intuitive. For example, Chou *et al* (2008) recently demonstrated that deletion of the gene encoding the repressor Dig2 led to a decrease rather than an increase in pheromone-induced transcription. Therefore, we sought to combine mathematical modeling with experimental investigations to understand how this system regulates transcription to ensure that the correct genetic program is followed.

Our investigations led to the discovery of two novel functions for the negative regulators Dig1 and Dig2. In addition to inhibiting Ste12, Dig1 and Dig2 protect the transcriptional activator from degradation. This protective binding ensures a large pool of inactive Ste12 is present prior to pheromone stimulation and allows the system to respond rapidly once a signal is received. Additionally, we show that the protective binding naturally generates a transient response to a sustained pheromone exposure with the amount of active Ste12 eventually returning exactly to its prestimulus level (perfect adaptation). We use a reduced version of the model to demonstrate how this adaptive behavior is achieved without the need for additional forms of negative regulation.

Results

Dig2 positively regulates pheromone-induced gene expression

Recently Chou *et al* (2008) reported that deletion of *DIG2* leads to a decrease in pheromone-induced transcription from the prototypical mating gene, *FUS1*. This result is surprising because deletion of a repressor is expected to increase, not decrease, transcriptional output. To confirm this finding, we compared pheromone-stimulated *FUS1* reporter gene activity in a *dig2*Δ strain to that in the wild-type (*WT*) strain using a standard β-galactosidase assay (Figure 1A). Consistent with the previous report, *dig2*Δ cells showed diminished pheromone-induced expression from the *FUS1* reporter gene. We then assessed whether Dig2 has a positive effect on mating differentiation based on the morphological change in vegetative cells that occurs as pheromone induces the formation of mating projections (Figure 1B). Cultures of the *WT* strain treated with pheromone had more cells that formed mating projections than did cultures of the *dig2*Δ mutant strain (Figure 1C). These results further show that transcriptional regulation by Dig2 has an effect on the physiological changes required for mating.

A model for transcriptional regulation by Ste12

We first considered two simple mechanisms that could explain the transcriptional effects seen in the *dig2*Δ mutant. Tec1 and Dig2 compete for the same binding site on Ste12 (Chou *et al*, 2006). Therefore, a potential mechanism for Dig2's positive role in transcriptional induction is that Dig2 prevents the formation of Ste12–Tec1 heterodimers, providing a larger pool of Ste12 multimers for activation of the mating transcriptional program. However, Chou *et al* (2008) found that Dig2's positive effect on transcription is independent of Tec1, eliminating this possibility. A second way that Dig2 could have a positive role in transcription would be for Dig2 to protect Ste12 from degradation. Such protection would increase the steady-state amount of Ste12 that is available and allow for a related increase in transcription upon pheromone stimulation. To test this mechanism we built a simple model to simulate *FUS1* mRNA induction involving only Ste12 and Dig2 (Figure 2, red components). In this model, Ste12 is not degraded when in a complex with Dig2. Pheromone stimulation causes phosphorylation of Dig2 and its subsequent dissociation from the Ste12. The free Ste12 then activates transcription of genes, including *FUS1*. This simple model predicts that *FUS1* mRNA induction is greater in *WT* than *dig2*Δ strains. This qualitative agreement between the simple model and empirical determinations (above) supports

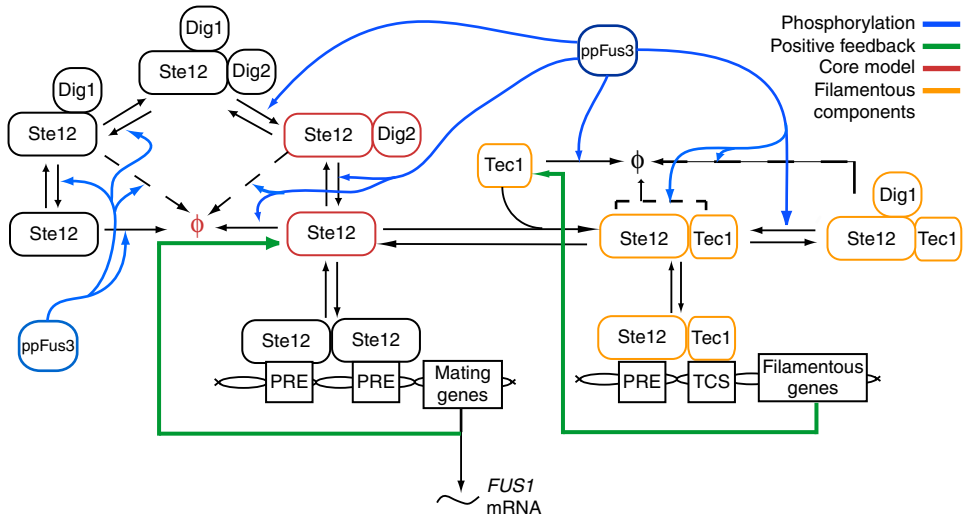

Figure 2 A model for transcriptional regulation by the pheromone response pathway. The elements of the pathway considered in the simple model are indicated in red. Components of the pathway leading to filamentation gene transcription are indicated in orange. Black arrows indicate transitions between the depicted complexes. Blue arrows indicate transitions that are accelerated by ppFus3-dependent phosphorylation. Green arrows indicate positive feedback loops, resulting in transcription of more Ste12 or Tec1. The empty set ϕ indicates component degradation.

the idea that Dig2-dependent protection of Ste12 is an important element of the transcriptional regulation mediated by Ste12.

Encouraged by the success of this preliminary model, we extended it by incorporating additional features based on what is currently known about the function and regulation of Ste12 (Figure 2). Ste12 activates transcription as either a homomultimer or as a heteromultimer with other transcriptional regulators such as Tec1. Ste12 homomultimers activate transcription of mating genes, which have multiplePREs in their promoters (Dolan *et al*, 1989; Olson *et al*, 2000). Ste12–Tec1 heterodimers activate transcription of filamentation genes, which have Tec1 consensus sequences (TCSs) or composite PRE–TCS elements in their promoters (Baur *et al*, 1997; Madhani and Fink, 1997). For simplicity, our model specifies transcriptional activation of mating genes by Ste12 homodimers binding to two PREs and activation of filamentation genes by Ste12–Tec1 heterodimers binding to PRE–TCS composite elements. *FUS1* mRNA is specified in the model as the transcriptional output of a typical mating gene (McCaffrey *et al*, 1987; Trueheart *et al*, 1987). The promoter region for *STE12* contains four PREs and that for *TEC1* contains a PRE–TCS composite sequence (Zeitlinger *et al*, 2003). Thus the model includes positive feedback loops for Ste12 and Tec1 (Figure 2, green arrows).

In the absence of pheromone, Ste12 homodimers are held in a repressed state by the negative regulators Dig1 and Dig2, whereas Ste12–Tec1 heterodimers are repressed by only Dig1 (Olson *et al*, 2000; Chou *et al*, 2006). Ste12 can bind to DNA if it is in a complex with Dig1 (inactive form; Zeitlinger *et al*, 2003) but Ste12 cannot bind to its promoter when it is in a complex with Dig2 (Olson *et al*, 2000). Thus, Ste12 in a complex with Dig1, but not Dig2, can compete with free and active Ste12 for binding sites on promoters.

Following stimulation with pheromone, the MAP kinases Fus3 and Kss1 phosphorylate Dig1 and Dig2 (Figure 2, blue arrows), causing the proteins to dissociate from Ste12, activating both Ste12 homodimers and Ste12–Tec1 heterodimers (Tedford *et al*, 1997). Active Fus3 also phosphorylates Tec1 and Ste12 (Figure 2, blue arrows) promoting their degradation (Chou and Liu, 2004; Bao *et al*, 2004; Bruckner *et al*, 2004; Esch *et al*, 2006). Pheromone-induced degradation of Tec1 contributes to the specificity of mating gene activation and that of Ste12 contributes to transient activation of mating genes and attenuation of the mating response.

A key premise of the model we developed is that the degradation rate for Ste12 depends on its oligomeric state. We assume Ste12 is most rapidly degraded when it is not part of a complex and include the possibility that its degradation rate varies with different binding partners (Figure 2, dashed arrows indicate the possibility of Ste12 degrading while it is in a complex with one or another of its binding partners). Another important feature of the model is that the kinetics of Ste12 degradation is saturable. That is, the rate at which Ste12 is degraded asymptotically approaches a maximum value as the abundance of Ste12 is increased. The rationale for including saturation effects is given below. These postulated features regarding Ste12 binding partners and degradation were incorporated along with known regulatory mechanisms (above) to develop a mathematical model of transcriptional regulation in the yeast pheromone response pathway based on ordinary differential equations (see Supplementary information for model equations, variable names, Supplementary Table S1, and parameter definitions and values, Supplementary Table S2).

Evaluation of the model

We used a Ste12–GFP fusion protein to experimentally measure abundance and degradation rates in different mutant strains to benchmark the model. We have previously documented the suitability of using a tagged version of Ste12 (Ste12–GST) for studies on Ste12 protein dynamics (Esch *et al*, 2006). To ensure that the addition of GFP to Ste12 did not alter

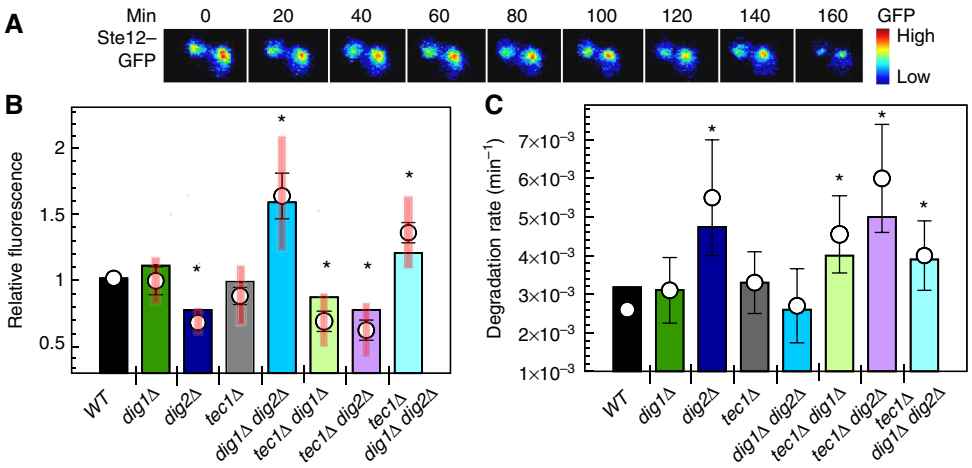

Figure 3 Comparison of Ste12 abundance and degradation rates in *WT* and mutant strains. (**A**) Micrographs showing the fluorescence intensity of Ste12–GFP following addition of a protein synthesis inhibitor (20-μM cyclohexamide) to *WT* cells. (**B**) Quantification of Ste12–GFP steady-state fluorescence (circles) and the corresponding model fit (bars) in *WT* and indicated mutant cells. Black error bars indicate standard error and thick red bars show standard deviation from the mean. (**C**) Ste12–GFP degradation rates (circles) and the corresponding model fit (bars) in *WT* and indicated mutant cells. Rates were determined from changes in fluorescence intensity of Ste12–GFP after inhibition of protein synthesis as in A. Black error bars indicate standard error. In both A and C, average values for each strain were determine from measurements on >100 cells. An asterisk above the error bars indicates that values are statistically different from the *WT* reference ($P<0.05$). Source data is available for this figure in the Supplementary Information.

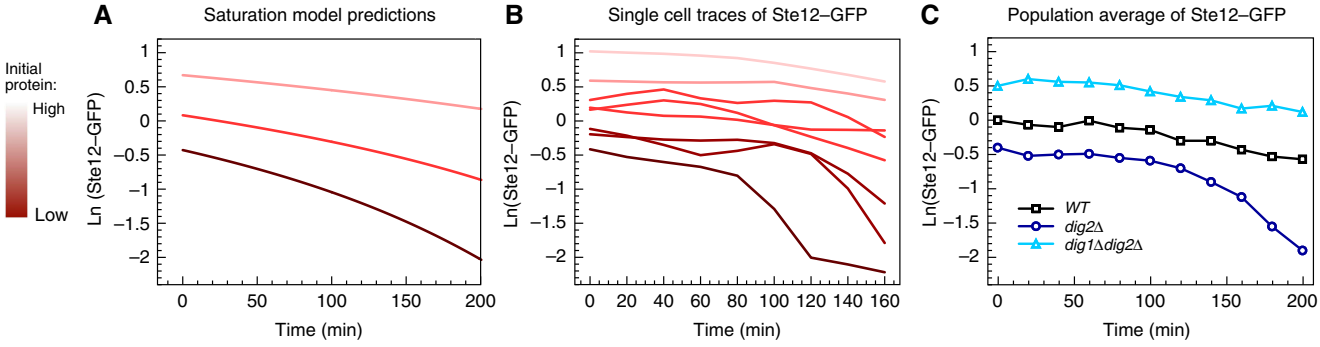

Figure 4 Saturating degradation kinetics. (**A**) Model predictions for degradation of Ste12 starting at different initial steady-state amounts. (**B**) Single cell traces of Ste12–GFP abundance in the *dig2*Δ strain before ($t=0$) and after inhibition of protein synthesis (cycloheximide, 20 μM). Traces show the dependence of Ste12–GFP degradation on the initial amount of Ste12 within a population. (**C**) Population average degradation curves for Ste12–GFP expressed in *WT* (black squares), *dig2*Δ (blue circles) and *dig1*Δ *dig2*Δ (cyan triangles) strains.

its degradation kinetics, we confirmed, using western blot methods, that the Ste12–GFP fusion degradation rate is similar to that measured for Ste12–GST (Supplementary Figure S3). To generate the necessary data sets, we constructed strains expressing Ste12–GFP from the endogenous *STE12* locus in *WT* and single, double, and triple *dig1*Δ, *dig2*Δ, and *tec1*Δ mutant strains. The Ste12–GFP fusion allowed for convenient estimation of the relative Ste12 abundance in each of these strains based on measurements of fluorescence intensity (Figure 3A). We measured the fluorescence of Ste12–GFP in early log-phase cells to determine the average steady-state amount in each of the specified strains (Figure 3B, open circles). To measure Ste12–GFP degradation rates, cultures were treated with the protein synthesis inhibitor, cycloheximide. Fluorescence measurements were made before ($t=0$) and at 20-min intervals for the next 180 min after addition of the inhibitor. The fluorescence time series from individual cells were averaged and fit to a decreasing exponential function to determine the 'effective' degradation rate per min for each of the specified strains (Figure 3C, open circles). The measured values are termed 'effective' rates because, in general, Ste12–GFP degradation does not follow first-order kinetics. First, the rate of Ste12 depletion is a function of multiple rate constants that depend on Ste12's binding partners. Second, we observed that Ste12–GFP degradation is subject to saturation (Figure 4). To mimic the experiments involving treatment with cycloheximide, for each strain considered, the model is run to steady state. The rate constants for protein synthesis are then set equal to zero, and the model is run to generate time series for the total Ste12 abundance. These time series are then used to compute the degradation rates reported in Figure 3C. Also included in the training data set was a time series for measurements of pheromone-induced *FUS1* mRNA abundance (Figure 5D, black data points). The inclusion of these data allowed us to estimate model parameters characterizing mRNA turnover and Fus3-mediated changes in the stability of Ste12 and Tec1 (see below for details).

Consistent with a mechanism in which Dig2 protects Ste12 from degradation, the *dig2*Δ strain showed a faster effective degradation rate and a decrease in Ste12 abundance as compared with the *WT* strain (Figure 3A and B). However, many of the other mutant strains produced results that were non-intuitive and initially seemed inconsistent with the model. For example, the effective Ste12 degradation rate in the *dig1*Δ *dig2*Δ-double mutant is similar to that of the *WT* reference rather than being the same or greater than that for the *dig2*Δ-single mutant. Yet the full model gave a good fit to the experimental data for this and the other mutant strains (Figure 3B and C, compare bars and circles, respectively). As discussed below, the ability of our model to capture these complex experimental results depends upon the nonlinear interplay between protective protein–protein interactions, positive feedback and saturating degradation kinetics.

In the case of the *dig1*Δ mutant, the effective degradation rate and steady-state abundance of Ste12 are unchanged compared with *WT*. The model accounts for the equivalence between mutant and *WT* because the loss of protection from the Ste12–Dig1 complex is compensated by an increase in the relative abundance of the Ste12–Tec1 complex (Table I). This shift favoring Ste12–Tec1 heterodimer formation in the *dig1*Δ mutant occurs because the Tec1-positive feedback loop is active, while the Ste12-positive feedback loop remains repressed. For the *tec1*Δ mutant, the degradation rate and steady-state abundance are also the same as for the *WT* reference. In this case, it is the low abundance of the Ste12–Tec1 heterodimer in the *WT* reference (Table I) that makes the absence of Tec1 in the deletion mutant a relatively neutral perturbation. The *dig2*Δ-single and *dig2*Δ *tec1*Δ-double mutants have a degradation rate that is increased for Ste12 and a steady-state abundance that is reduced compared with the *WT* reference. The model captures the change in degradation rate in the mutants because the major protective binding partner(s) is (are) missing. The positive feedback of Ste12 production is still kept low in both mutants due to repression by Dig1. Without compensation from positive feedback, the increased degradation rate causes a net decrease in Ste12 steady-state abundance. The *dig1*Δ *tec1*Δ-double mutant also has a higher effective degradation rate and lower Ste12 steady-state abundance than the *WT* reference. In this case, the trends are due to the combined loss of the stabilizing effects of Dig1 and Tec1 and repression of the Ste12-positive feedback loop by Dig2. The *dig1*Δ *dig2*Δ-double mutant shows an effective degradation rate that is comparable to *WT* rather than the *dig2*Δ-single mutant and a steady-state abundance that is increased compared with the *WT* reference. The model captured this behavior based on the increased pool of Ste12–Tec1 heterodimers (Table I), which are protected from degradation, and the effect that saturation has on degradation kinetics. The *dig1*Δ*dig2*Δ *tec1*Δ-triple mutant has a higher effective degradation rate and higher Ste12 abundance than the *WT* reference. Both trends are expected because of the loss of binding partners and the contribution from the Ste12-positive feedback loop, respectively. However, the complete loss of binding partners should have made the Ste12 degradation rate largest in the triple mutant compared with any of the double mutant strains. Yet the measured effective degradation rate is less than that for the *dig2*Δ *tec1*Δ strain. The model accounts for this apparently slower degradation rate by the saturation of degradation kinetics.

Saturating degradation kinetics

The assumption of a single exponential decay for Ste12 depletion is not strictly true in our model because the effective degradation rate of Ste12 depends on its various binding partners. Yet simply allowing for combinatorial degradation rates was inadequate for simulating the apparent stability of Ste12 in several of the mutants. We reasoned that protein degradation in this system is an enzymatically driven process. Therefore, saturation effects are possible and the degradation rate could be concentration dependent.

The simplest way to include saturating effects in the degradation rate is to assume Michaelis–Menton kinetics (Supplementary information). Under this assumption, the degradation rate has the form $V_{\max} X/(K_m + X)$, where X is the total amount of substrate available for degradation. The maximum degradation rate $V_{\max}$ is approached as X increases and the Michaelis constant K_m determines the substrate concentration at which the degradation rate is half its maximum value. It is possible that protein degradation follows more complicated kinetics. However, our experimental data and modeling studies do not indicate a need for higher order kinetics. If protein synthesis is blocked, this model predicts an initial linear degradation regime that becomes exponential when the abundance of Ste12 is small compared with K_m. If the fluorescence time series is plotted on a semi-log scale and the effective degradation rate constant estimated using a linear fit to the data, the estimated value will be approximately $V_{\max}/(K_m + \langle X \rangle)$, where $\langle X \rangle$ is the time average concentration of Ste12 over the degradation time course. That is, the effective

Table I Predicted concentration and distribution of Ste12 in different genetic backgrounds

	Total Ste12 (nM)	Ste12–Ste12	Ste12–Dig1	Ste12–Dig2	Ste12–Dig1–Dig2	Ste12-Tec1	Ste12–Tec1–Dig1	Ste12	Ste12*[a]
WT	415	0	11	0	24	0	2	0	63
*dig1*Δ	455	0	0	20	0	21	0	0	59
*dig2*Δ	312	0	13	0	0	0	2	0	85
*dig1*Δ*dig2*Δ	667	3	0	0	0	23	0	1	73
*tec1*Δ	405	0	10	0	25	0	0	0	65
*tec1*Δ*dig1*Δ	355	0	0	22	0	0	0	0	78
*tec1*Δ*dig2*Δ	305	0	15	0	0	0	0	0	85
*tec1*Δ*dig1*Δ*dig2*Δ	504	5	0	0	0	0	0	1	94

[a]Ste12* includes all species on the pathway to degradation.

degradation rate constant decreases with increased Ste12 abundance (Figure 4A). Increasing the initial protein concentration increases the time it takes for degradation to show true exponential decay characterized by an effective rate constant of V_{max}/K_m (Figure 4A). Because of cell-to-cell variability in Ste12 steady-state abundance, the time to transition from the linear (in this case, flat on semi-log scale) to exponential (linear on semi-log scale) phase of degradation differs among individual cells present in the population of a single strain. This trend is shown for time series measurements of Ste12–GFP in individual *dig2*Δ cells after addition of a protein synthesis inhibitor (Figure 4B). The two regimes characteristic of saturating effects are also clearly apparent in population average degradation curves for Ste12–GFP in the *WT*, *dig2*Δ and *dig1*Δ *dig2*Δ strains (Figure 4C). These results validate incorporating saturating degradation kinetics into the model of transcriptional regulation in the pheromone response pathway. They demonstrate that estimating degradation kinetics from experimental data must be done with care.

Model validation

Our model contains two positive feedback loops formed through the autoregulation of Ste12 and Tec1. The effects of the Ste12-positive feedback loop can be seen in the results for the Ste12 abundance for *dig1*Δ *dig2*Δ *tec1*Δ-triple deletion mutant (Figure 5B). A key prediction of the model is that the Tec1-positive feedback loop is active in the *dig1*Δ mutant generating high basal levels of Tec1 (Figure 5B). To test this prediction we constructed a Tec1–GFP fusion in both a *WT* and *dig1*Δ background. We measured, approximately, a six-fold increase in Tec1 expression in the *dig1*Δ mutant compared with the *WT* strain confirming the model's prediction (Figure 5B).

To further test the model we investigated its ability to predict temporal profiles for pheromone induction of *FUS1* mRNA in several of the mutant strains (*dig1*Δ, *dig2*Δ, *dig1*Δ *dig2*Δ). As input to the model, we used a temporal profile for active Fus3 (ppFus3) consistent with experimental measurements made at 10 μM concentration of pheromone (see Supplementary information for details; Hao *et al*, 2008). Recall that the temporal profile for *FUS1* mRNA in the *WT* strain was included in the training data set. The model accurately captured key features of this time series, including the transient response with incomplete recovery to basal levels (compare Figure 5C and D, black curves). A strong prediction of our model is that the amplitude of *FUS1* mRNA induction will be less in the *dig2*Δ mutant compared with the *WT* reference (Figure 5C, blue and black curves). Although Ste12 steady-state abundance in the *dig1*Δ mutant is comparable to that of the *WT* strain (Figure 3A, $t=0$), the model predicts *FUS1* mRNA induction has a greater amplitude and more sustained profile in the mutant compared with the *WT* reference (Figure 5C, green and black curves). This profile results in part because the mutant eliminates competition between active Ste12 homodimers and the Ste12–Dig1 complex for PRE binding sites. Additionally, Tec1-positive feedback is active in the *dig1*Δ mutant. The stabilizing effect of Tec1 on Ste12 maintains Ste12 abundance, allowing transcription from mating genes following pheromone-induced degradation of Tec1. Finally, the model predicts that the *dig1*Δ *dig2*Δ mutant will have a significantly increased and more sustained transcriptional response than *WT* (Figure 5C, cyan and black curves). In this mutant, the lack of repression allows both positive feedback loops to operate in the absence of pheromone. Consequently, prior to pheromone induction, most of the Ste12 pool is bound to Tec1 and protected from degradation. Nevertheless, there are enough Ste12 homodimers to increase basal amounts of *FUS1* mRNA (Figure 5C). Following pheromone stimulation, Tec1 is degraded generating an increased pool of Ste12 homodimers that promotes transcription of *FUS1* mRNA.

To evaluate these model predictions, we used quantitative PCR to measure *FUS1* mRNA in the mutant strains before and at specified times following treatment with pheromone (Figure 5D). The experimental data for each of the strains generate profiles that are in good agreement with those predicted by the model. Specifically, the data illustrate the same relative amplitudes and attenuation features of the predicted profiles for the mutant strains compared with the *WT* reference. The data also illustrate the high basal expression characteristic of the *dig1*Δ *dig2*Δ mutant that was captured by the model. Another noteworthy feature is that the transient

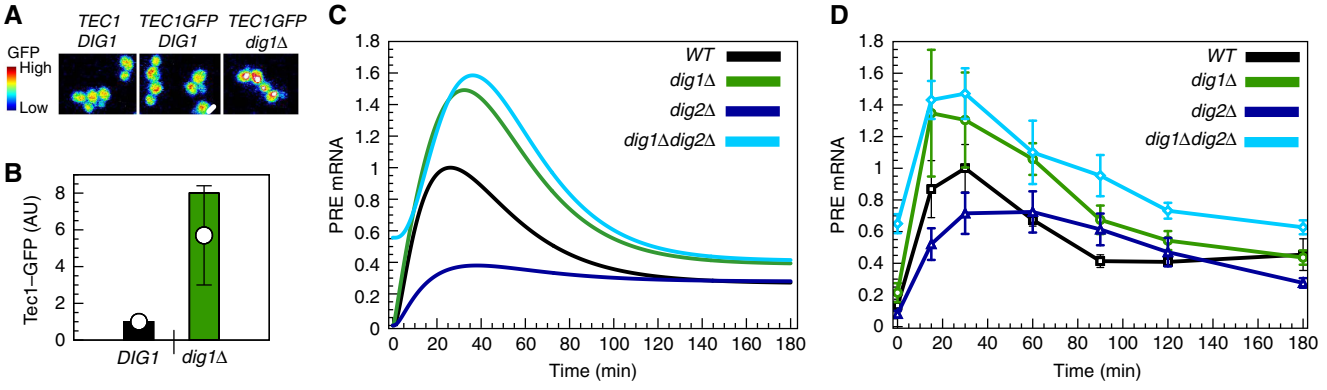

Figure 5 (**A**) Micrographs comparing fluorescence in *TEC1* (background fluorescence only). *TEC1GFP DIG1* and *TEC1GFP dig1*Δ cells demonstrating that Tec1–GFP is strongly induced in the *dig1*Δ mutant compared to *WT*. (**B**) Model predictions, bars and quantification of Tec1–GFP in *WT* and *dig1*Δ cells, open circles. *FUS1* mRNA profiles following pheromone stimulation. (**C**) Model predictions for *FUS1* mRNA temporal profiles. (**D**) Experimental measurements of mRNA in *WT*, *dig1*Δ, *dig2*Δ, *dig1*Δ *dig2*Δ cells. Source data is available for this figure in the Supplementary Information.

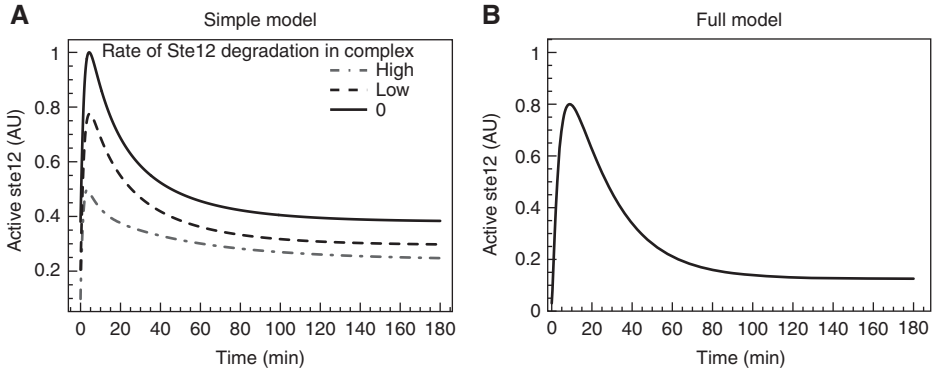

Figure 6 A mechanism for perfect adaptation. (**A**) Results for the simple model shown in red in Figure 2. The degree of adaptation is determined by the stability of Ste12 when bound to Dig2 (no degradation—black curve, bound Ste12 degrades at 30% the rate of the monomer—dashed line, 100% of Ste12 monomer—gray dot-dashed curve). (**B**) Results for the full model in which Ste12 degrades slowly when in protein–protein complexes.

transcriptional profiles peak 15–30 min after exposure to pheromone in contrast to MAPK kinase activity, which typically peaks at ~60 min. This offset is indicative that upstream signaling events cannot account for the transient transcriptional response. The model captures this transient profile without containing any negative feedback loops. One possible explanation for this behavior is the incoherent feed forward loop formed by Fus3-mediated degradation of Ste12. However, eliminating this effect from the model did not abrogate the transient response. We demonstrate below how protein–protein interactions that stabilize the binding partners naturally lead to robust perfect adaptation. In the Supplementary information section we present parameter studies to demonstrate the robustness of other key modeling results to the choice of parameter values.

Protective complexing leads to perfect adaptation

As noted above, the model naturally produces a transient transcriptional response on a time scale that is faster than the attenuation of MAPK activity without an explicit negative feedback loop. Analysis of the full model revealed that adaptation of Ste12 transcriptional output arises because the model is capable of robust perfect adaptation (Figure 6A). Robust perfect adaptation refers to the situation in which a sustained stimulus generates a transient response that eventually returns exactly to prestimulus levels independent of the kinetic parameters. We developed the simple model (Figure 2, red components) to illustrate how transcriptional regulation by Dig2 naturally leads to perfect adaptation (Figure 6A). The model Equations for this system are as follows:

$$\frac{dS_2}{dt} = a - \delta S_2 - k_1 S_2 D + (k_2 + s)C$$

$$\frac{dC}{dt} = k_1 S_2 D - (k_2 + s)C$$

where S_2 represents Ste12 homodimers, D represents Dig2 and C is the complex with Dig2 bound to the Ste12 homodimer. The parameters 'a' and 'δ' are the synthesis and degradation rate of Ste12, respectively, k_1 and k_2 are the binding and dissociation rates, respectively, in the absence of signal and 's' is the increase in the dissociation rate following pheromone stimulation. This model assumes that the total Dig2 concentration, $\mathrm{Dig2}_{\mathrm{total}} = D + C$ remains constant. It is straightforward to show that the steady state of S_2 is always independent of the stimulus, s (specifically the steady state is $S_2 = a/\delta$) regardless of the parameters values, demonstrating the system shows robust perfect adaptation. An advantage of this mechanism of adaptation is that it allows transcriptional induction to act on a shorter time scale than upstream MAP kinase activity. In the full model (Figure 2), active Ste12 homodimers do not return to prestimulus levels (see Figure 6B). The reason for this is that allowing degradation in the protective complexes ('C' in the simple model above) breaks the perfect adaptation. The more Ste12 degradation that is allowed to occur while in the complex, the more Ste12 post adaptation levels will be above the prestimulus amount (Figure 6A).

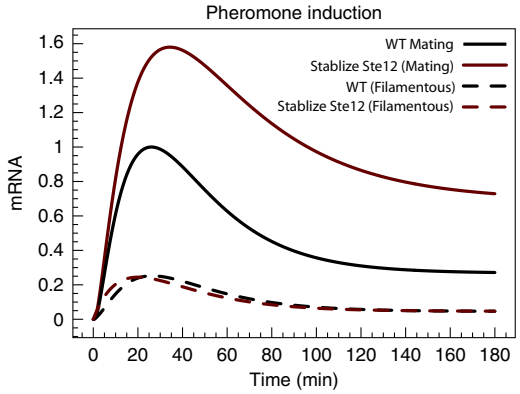

Figure 7 Predicted mRNA profiles. Model results for *FUS1* mRNA time series for a hypothetical mutant in which pheromone-dependent degradation of Ste12 through Fus3 phosphorylation is blocked (solid brown curve). The *WT* response is replotted from Figure 5 for comparison (black curve). Also shown are predicted profiles of expression from a promoter containing a TCS–PRE composite element (*WT*—black dashed curve, mutant—dashed brown curve).

The pheromone pathway contains an additional mechanism for damping transcriptional induction, in which Ste12 is degraded in a pheromone-dependent manner (Esch *et al*,

2006). This mechanism requires phosphorylation of Ste12 by Fus3. To investigate the relative roles of this mechanism and protective complexing in damping the transcriptional response, we used the model to simulate a hypothetical mutant in which Fus3 phophorylation of Ste12 is disrupted (Figure 7—brown solid curve). Our model predicts that Fus3-mediated degradation of Ste12 primarily serves to dampen the overall transcriptional response (Figure 7—compare brown solid curve with black solid curve). In both the *WT* and mutant strain, the formation of protective Ste12 complexes is sufficient to produce a transient response. Because phosphorylation of Tec1 by Fus3 increases degradation of this transcription factor, disrupting phosphorylation of Ste12 only has a small effect on expression from promoters containing a TCS–PRE composite element (Figure 7—dashed curves).

Discussion

Genetic regulatory networks often contain multiple control mechanisms that tightly coordinate gene expression. In the yeast pheromone response, the transcriptional activator Ste12 is subject to both positive feedback through promotion of its own synthesis and negative regulation by transcriptional repressors and pheromone-induced degradation. Here we have demonstrated an additional regulatory mechanism in which Ste12's stability is increased through protein–protein interactions with other transcriptional regulators. Additionally, we have presented data demonstrating that Ste12's degradation follows saturation kinetics. We developed a mathematical model to understand how these nonlinear effects interact to generate an appropriate mating response. The mathematical model was able to reproduce the often counterintuitive experimental data for the abundance and stability of Ste12 obtained by selectively deleting components of the regulatory system. As evidence for the validity of the model, it accurately predicted the qualitative behavior of the temporal profile of pheromone-induced transcription of the mating-specific gene *FUS1* in several of the different genetic backgrounds.

Our modeling revealed a novel regulatory motif for perfect adaptation, a property of certain signaling pathways in which a subset of the signaling components eventually return precisely to their basal activity levels in the presence of persistent input signal. Adaptive responses typically involve negative feedback or feed forward regulation (Yi *et al*, 2000; Sontag, 2003). In our model, the mechanism for perfect adaptation involves stabilization through protein–protein interactions. In the context of the yeast mating response, the increased stability of Ste12 when associated with the transcriptional repressors Dig1 and Dig2 also ensures that prior to pheromone stimulation a large, but repressed, pool of Ste12 exists. This pool can then be rapidly activated once an appropriate signal is received. The perfect adaptation of this regulatory motif allows cells to mount a transcriptional response that is on a shorter time scale than the kinetics of upstream MAP kinase activity. During the pheromone response, the MAP kinase Fus3 has multiple functions. It is not only responsible for regulating gene expression, but also is required for cell cycle arrest and gradient sensing. These processes happen on different time scales necessitating multiple control mechanisms. An additional advantage of using the protective interaction motif as a mechanism for adaptation is that the level of adaptation can be tuned through the degradation rate of the protected complex. If Ste12 is completely stable when part of a protein–protein complex, the system is perfectly adapting. In general, however, the level of adaptation is determined by the relative stability of the Ste12 complex (Figure 6A). Tightly regulating Ste12 abundance is important because overexpression of Ste12 has been shown to have deleterious effects (Dolan *et al*, 1989).

We have shown how stabilizing protein–protein interactions can modulate transcriptional, as well as biological outcomes in the yeast mating response. Because stabilizing protein–protein interactions have been observed in other diverse contexts, we expect that the principles discussed in this paper could be important in a wide variety of circumstances. For instance, the transcriptional repressor Matα2 is stabilized through interactions with the co-repressors Tup1 and Ssn6 (Laney *et al*, 2006). The protected fraction is engaged in repressing **a**-specific genes and is small compared with the unprotected fraction that is rapidly degraded. Laney *et al* (2006) proposed that this situation accommodates the opposing requirements that the Matα2 imposes the **α**-cell type identity by repressing **a**-specific genes and yet is still sufficiently short lived for cells to rapidly change cell-type identity upon mating-type switching. Increased stability through protein–protein interactions has a role in signal transduction beyond transcriptional regulation. For example, one study (Boutler *et al*, 2010) demonstrated that Rho GDI1 which binds to multiple Rho GTPases also slows their degradation producing an increased pool of these proteins. The existence of protective complexes in these two other systems highlights the potential generality of this regulatory motif in signal transduction.

Materials and methods

Yeast strains, genetic procedures and growth conditions

Yeast strains used in this study are isogenic with BY4741 or BY4742 and are listed in Supplemental Table S4 (Brachmann *et al*, 1998). Media preparation and standard yeast genetic methods for transformation, gene replacement, crosses and tetrad dissection were as described in Amberg *et al* (2005). Details of the strain constructions are provided in Supplementary information.

Reporter gene assay

Expression of the *FUS1-lacZ* reporter gene was assessed by measuring the amount of β-galactosidase activity in yeast whole-cell extracts as described previously (Hoffman *et al*, 2002). We measured, with two independent replicates, induction of *FUS1-lacZ* by 10 μM alpha factor in *WT* and *dig2*Δ mutants.

Mating response assay

Mating response was assessed based on the accumulation of cells in pheromone-treated cultures with mating projections (shmoo morphology). Five ml cultures of specified strains were grown in synthetic complete medium with dextrose (SCD) to approximately 0.5×10^7 cells/ml. A volume of 400 μl of each culture was removed to an eppendoph tube at $t = 0$, cells were sonicated mildly to disperse clumps, and cells were counted and scored for budding index using a

hemacytometer. Pheromone was added to a final concentration of 10 μM. A volume of 400 μl samples were taken from each sample at 60 min intervals and sonnicated. Cells were counted and scored for vegetative and pheromone-induced morphological changes using a hemacytometer. Imaging of representative samples from these cultures was performed with a Nikon TE 2000 inverted microscope using a Hammatsu OrcaII Monochrome camera. Acquisition was performed with Metamorph software (Molecular Devices; http://www.photomet.com). Image processing and cell scoring were aided by use of ImageJ software (http://rsbweb.nih.gov/ij/).

Fluorescence measurements and quantification

Nuclear fluorescence from Ste12–GFP strains was quantified using an epifluorescent microscope (Nikon TE 2000 inverted microscope) using a Hammatsu OrcaII Monochrome camera. Five-ml cultures were grown in synthetic complete medium with dextrose (SCD) to approximately 0.5×10^7 cells/ml (early-log phase). A small portion of the cells were placed on a pad made of 4% agarose in SCD medium, formed on a glass slide. Cells on this medium were held at 30°C for the duration of the experiment. All experiments measuring degradation were done with 20 μg/ml cyclohexamide (where applicable). To measure fluorescence, 1-s exposures were taken at several different equally spaced planes that spanned the cell from top to bottom. The resulting image stack was then projected on to the same plane by adding the individual planes together. The background fluorescence was subtracted using a standard background subtraction algorithm in ImageJ. (http://rsbweb.nih.gov/ij/). Ste12–GFP was clearly visible inside the nucleus. To quantify the total fluorescence, we drew a circle around the nucleus of Ste12–GFP-expressing cells and integrated the intensity. Quantification of nuclear fluorescence was aided by an edge detection algorithm written in MATLAB (Mathworks) based on an implementation of the Hough transform used by Nachman *et al* (2007). Average autofluorescence, per pixel, was estimated by measuring fluorescence of cells that were not expressing GFP. The autofluorescence per pixel was then multiplied by the number of pixels measured for a particular cell and subtracted from the measurement for that cell's intensity. For time course measurements, we took images of the fluorescing cells every 20 min, keeping the temperature constant at 30°C. For Figures 3A and 5A, the ImageJ '16 colors' LUT was used for ease of visualization. For Figure 4B, individual cells were tracked in time, using a custom Matlab script, by finding the minimum geometric distance between cells in one frame to the next. A moving average filter using three time points was then applied to each cell individually to help smooth measurement error. To ensure that we were not bleaching our GFP signal, we took pictures of cells that had not previously been exposed to light at the end of the experiment and on the same agarose pad. After quantification we compared the average Ste12–GFP from cells exposed only once and cells exposed over the whole time course. We found no significant difference between the two populations, indicating that bleaching is not significant for our experiments.

RNA preparation and quantification of *FUS1* mRNA

Yeast cultures for RNA preparation were grown at 30°C in YPD to 1×10^7 cells/ml. Ten-ml samples were removed from the culture immediately before and at indicated times after addition of mating pheromone (10 μM α-factor). Cells were collected from these samples by vacuum filtration on to filters (0.45 μm HAWG, Millipore). The filters were placed in 1.5-ml eppendorf tubes, cooled in a dry ice/ethanol bath and stored at −80°C until all samples were collected for RNA extraction.

Total RNA was extracted from each sample using a modified version of the hot acidic phenol–chloroform method developed by Collart and Oliviero (2001). After adding 400 μl of TES buffer (10 mM Tris–HCl (pH 7.5), 10 mM EDTA, 0.4% SDS, 4% RNA*secure* (Ambion Inc.)) to each tube, the samples were briefly vortexed and centrifuged to separate the suspended cells from the filters, which were then discarded. A volume of 400 μl of phenol, pH 4.5 (MP), was added to each cell suspension. Samples were vortexed vigorously, incubated at 65°C for 1 h with intermittent vortexing, and then placed on ice for 5 min. Each mixture was applied to a phase-lock gel tube (5 Prime) to separate the aqueous and organic phases by centrifugation. The aqueous phase was removed to a clean phase-lock tube and extracted with an equal volume of chloroform. The aqueous phase was transferred to a clean eppendorf tube and ethanol precipitated. The precipitated RNA samples were suspended in 100-μl RNase-free water. The quality and concentration of the RNA for subsequent real-time quantitative PCR (qPCR) analysis was assessed based on 260/280 nm and 260/230 nm absorbance ratios.

First-strand cDNA synthesis for qPCR analysis was generated from total RNA using the SuperScript® III First-Strand Synthesis System (Invitrogen). qPCR reactions using 1/20 of total cDNA as template were completed using primers specific to *FUS1* mRNA and the *ACT1* reference mRNA (Supplementary Table S5). qPCRs were carried out in triplicate for each cDNA sample using SYBR GreenER qPCR supermix (Invitrogen) and the Applied Biosystems 7900HT Fast Real-Time PCR system. Reported values for amounts of *FUS1* mRNA are the average of determinations made on samples from three replicate cultures.

Modeling

We sought to model degradation of Ste12 with and without pheromone induction as well as transcription of a mating-specific gene (*FUS1*), which is solely dependent on Ste12. To do this we used as input ppFus3, and built an ODE model to compute concentrations, using mass action kinetics, and Tables S1 and S2 for Ste12, Tec1, Ste12–Dig1, Ste12-Dig2, Ste12–Dig1-Dig2, Ste12–Tec1, Ste12–Tec1-Dig1, mating-specific gene mRNA and filamentation specific gene mRNA. See Supplementary information and Supplementary Tables S1 and S2 for the full set of equations and parameters used. Additionally, this model is deposited in the Biomodels database (accession number MODEL1204040000). ODEs were solved using an implementation of the Runge–Kutta algorithm in Matlab. Because most of the parameters are unknown, initial parameters were chosen using what we deemed to be reasonable estimates. To fit the model to the benchmark data, we iteratively did random parameter searches, chose the best fitting parameter set, tuned by hand to get a better fit, and then again searched randomly near that region. To help reduce the dimensionality of our model we used a quasi-equilibrium approximation for promoter activation. This is reasonable as the binding of transcription factors to their promoters on DNA is often relatively fast.

Supplementary information

Supplementary information is available at the *Molecular Systems* Biology website (www.nature.com/msb).

Acknowledgements

We thank H Dohlman and J Kelly for critical reading of the manuscript and valuable discussions. This work was supported by NIH grants GM-084071 (JRH, EF, BE, TCE) and GM-079271 and GM-073180 (TCE).

Author contributions: JRH developed the model and performed the analyses and computational simulations. JRH, EF, MJN and BE performed the experiments and analyzed the data. TCE provided guidance on modeling, while BE gave guidance on the design of experiments. JRH, TCE and BE wrote the manuscript. All authors gave intellectual input and comments on the manuscript.

Conflict of Interest

The authors declare that they have no conflict of interest.

References

Amberg DC, Burke D, Strathern JN, Cold Spring Harbor Laboratory (2005). *Methods in Yeast Genetics: A Cold Spring Harbor Laboratory*

Course Manual, 2005 edn. Cold Spring Harbor, NY: Cold Spring Harbor Laboratory Press

Bao MZ, Schwartz MA, Cantin GT, Yates JR 3rd, Madhani HD (2004) Pheromone-dependent destruction of the Tec1 transcription factor is required for MAP kinase signaling specificity in yeast. *Cell* **119:** 991–1000

Bardwell L, Cook JG, Zhu-Shimoni JX, Voora D, Thorner J (1998) Differential regulation of transcription: repression by unactivated mitogen-activated protein kinase Kss1 requires the Dig1 and Dig2 proteins. *Proc Natl Acad Sci USA* **95:** 15400–15405

Baur M, Esch RK, Errede B (1997) Cooperative binding interactions required for function of the Ty1 sterile responsive element. *Mol Cell Biol* **17:** 4330–4337

Boulter E, Garcia-Mata R, Guilluy C, Dubash A, Rossi G, Brennwald PJ, Burridge K (2010) Regulation of Rho GTPase crosstalk, degradation and activity by RhoGDI1. *Nat Cell Biol* **12:** 477–483

Brachmann CB, Davies A, Cost GJ, Caputo E, Li J, Hieter P, Boeke JD (1998) Designer deletion strains derived from *Saccharomyces cerevisiae* S288C: a useful set of strains and plasmids for PCR-mediated gene disruption and other applications. *Yeast* **14:** 115–132

Bruckner S, Kohler T, Braus GH, Heise B, Botle M, Mosch HU (2004) Differential regulation of Tec1 by Fus3 and Kss1 confers signaling specificity in yeast development. *Curr Genet* **46:** 331–342

Chou S, Huang L, Liu H (2004) Fus3-regulated Tec1 degradation through SCFCdc4 determines MAPK signaling specificty during mating in yeast. *Cell* **119:** 981–990

Chou S, Lane S, Liu H (2006) Regulation of mating and filamentation genes by two distinct Ste12 complexes in Saccharomyces cervisiae. *Mol Cell Biol* **26:** 4794–4805

Chou S, Zhao S, Song Y, Liu H, Nie Q (2008) Fus3-triggered Tec1 degradation modulates mating transciptional output during pheromone response. *Mol Syt Biol* **4:** 212

Collart MA, Oliviero S (2001) Preparation of yeast RNA. *Curr Prot Mol Biol* **Chapter 13:** Unit13 12

Cook JG, Bardwell L, Kron SJ, Thorner J (1996) Two novel targets of the MAPK kinase Kss1 are negative regulators of invasisve growth in the yeast *Saccharomyces cerevisiae*. *Genes Dev* **10:** 2831–2848

Dolan JW, Kirkman C, Fields S (1989) The yeast STE12 protein binds to the DNA sequence mediating pheromone induction. *Proc Natl Acad Sci USA* **86:** 5703–5707

Esch RK, Wang Y, Errede B (2006) Pheromone-induced degradation of Ste12 contributes to signal attenuation and the specificity of developmental fate. *Eukaryot Cell* **5:** 2147–2160

Hao N, Nayak S, Behar M, Shanks RH, Nagiec MJ, Errede B, Hasty J, Elston TC, Dohlman HG (2008) Regulation of cell signaling dynamics by the protein kinase-scaffold Ste5. *Mol Cell* **30:** 649–656

Hoffman GA, Garrison TR, Dohlman HG (2002) Analysis of RGS proteins in *Saccharomyces cervisiae*. *Methods Enzymol* **344:** 617–631

Laney JD, Mobley EF, Hochstrasser M (2006) The short-lived Matalpha2 transcriptional repressor is protected from degradatoin in vivo by interactions with its corepressors Tup1 and Ssn6. *Mol Cell Biol* **26:** 371–380

Madhani HD, Fink GR (1997) Combinatorial control required for the specificity of yeast MAPK signaling. *Science* **275:** 1314–1317

McCaffrey G, Clay FJ, Kelsay K, Sprague Jr GF (1987) Identification and regulation of a gene required for cell fusion during mating of the yeast *Saccharomyces cerevisiae*. *Mol Cell Biol* **7:** 2680–2690

Nachman I, Regev A, Ramanathan S (2007) Dissecting timing variability in yeast meiosis. *Cell* **131:** 544–556

Olson KA, Nelson C, Tai G, Hung W, Yong C, Astell C, Sadowski I (2000) Two regulators of Ste12p inhibit pheromone-responsive transcription by seperate mechanisms. *Mol Cell Biol* **20:** 4199–4209

Roberts CJ, Nelson B, Marton MJ, Stoughton R, Meyer MR, Bennett HA, He YD, Dai H, Walker WL, Hughes TR, Tyers M, Boone C, Friend SH (2000) Signaling and circuitry of multiple MAPK pathways revealed by a matrix of global gene expression profiles. *Science* **287:** 873–880

Sontag E (2003) Adaptation and regulation with signal detection implies internal model. *Syst Contr Lett* **50:** 119–126

Tedford K, Kim S, Sa D, Stevens K, Tyers M (1997) Regulation of the mating pheromone and invasive growth responses in yeast by two MAP kinase substrates. *Curr Biol* **7:** 228–238

Trueheart J, Boeke JD, Fink GR (1987) Two genes required for cell fusion during yeast conjugation: evidence for a pheromone-induced surface protein. *Mol Cell Biol* **7:** 2316–2328

Yi TM, Huang Y, Simon MI, Doyle J (2000) Robust perfect adaptation in bacterial chemotaxis through integral feedback control. *Proc Natl Acad Sci USA* **97:** 4649–4653

Zeitlinger J, Simon I, Harbison CT, Hannett NM, Volkert TL, Fink GR, Young RA (2003) Program-specific distribution of a transcription factor dependent on partner transcription factor and MAPK signaling. *Cell* **113:** 395–404